Journal of Power Sources 256 (2014) 336–344

Contents lists available at ScienceDirect

Journal of Power Sources

journal homepage: www.elsevier.com/locate/jpowsour

Hierarchical carbon-coated $LiFePO_4$ nano-grain microspheres with high electrochemical performance as cathode for lithium ion batteries

Yi-Fang Wu [a,b], Yong-Ning Liu [a,*], Sheng-Wu Guo [a], Sheng-Nan Zhang [b], Tian-Ni Lu [a,b], Ze-Ming Yu [b], Cheng-Shan Li [b], Zheng-Ping Xi [a,b,*]

[a] State Key Laboratory for Mechanical Behavior of Materials, Xi'an Jiaotong University, Xi'an 710049, China
[b] Northwest Institute for Nonferrous Metal Research, 96 Weiyang Road, Xi'an 710016, China

HIGHLIGHTS

- Hierarchical nano-grains $LiFePO_4$/C microspheres were got by co-precipitation method.
- Micron-sized spheres are good for tap density; nano-grains help for Li-ion diffusion rate.
- It shows high discharge capacity and excellent cycling stability as cathode.
- The rate capacities increased by electric conductivity are more obvious than Li-ion diffusion rate.

ARTICLE INFO

Article history:
Received 5 November 2013
Received in revised form
26 December 2013
Accepted 8 January 2014
Available online 17 January 2014

Keywords:
Lithium iron phosphate
Nano
Co-precipitation
Electrochemical
Hierarchical

ABSTRACT

The hierarchical carbon-coated $LiFePO_4$ nano-grain microspheres are prepared by a chemical co-precipitation method. The microstructure and electrochemical properties of $LiFePO_4$/C composites treated at 950–1025 K are intensively investigated. The rate discharge capability has been obviously enhanced when sample is treated at 1025 K. This attributes to its improved electric conductivity of 0.09 S cm^{-1} due to the in-situ formation of Fe_2P phase. The cycling stabilities are excellent until 300 cycles for all the samples at the rate 1C in discharge, which is very difficult to reach for nano-grains with large specific surface area and high reaction activity. Our samples with hierarchical microstructures exhibit high Li-ion diffusion rate (10^{-9}–10^{-13} cm^2 S^{-1}) with enhanced tap density (1.30 g cm^{-3}). It is considered in our paper that the rate capacities increased by Li-ion diffusion rate are not as obvious as electric conductivity. Therefore, the $LiFePO_4$/$FePO_4$ reaction is a non-diffusional controlled process.

1. Introduction

$LiFePO_4$ is one of the primary battery materials for electric vehicle (EV) applications [1]. The main advantages of $LiFePO_4$ are its preeminent safety, flat voltage profile, low material cost, and better environmental compatibility compared to other cathode materials [2–7]. The drawbacks of $LiFePO_4$ include its low tap density, poor electronic conductivity and low ionic diffusivity. Moreover, the processing cost of $LiFePO_4$ is generally high because carbon coating or small particle size is required to obtain appropriate performance at high current rates [8].

The poor electronic conductivity of $LiFePO_4$ can be improved by the in situ generation of a nano-network of conductive iron phosphide and carbon [9]. But the low Li-ion diffusive rate of $LiFePO_4$ has not been solved until now. The publicly accepted opinion is to achieve nano-scale $LiFePO_4$ grains to decrease the Li-ion diffusive distance between $LiFePO_4$ grains. However, The nano-sized $LiFePO_4$ materials have a lower tap density compared to micron-sized $LiFePO_4$. As we know, a positive electrode material of high tap density could reach a high volumetric capacity of the cell, which makes the tap density an increasingly important parameter in battery applications where the amount of inner space is highly limited.

Recently, the organization of nanoscale building blocks [10–30] into hierarchical architectures is of great interest to overcome the problems that occur in various electrochemical systems. Saravanan and coworkers [28,29] recently developed hierarchical carbon-coated $LiFePO_4$/C nanoplates. These desired three-dimensional hierarchical nanostructures exhibited better rate capability and considerable reversible capacity in comparison with the samples without hierarchical nanostructures. Meng Wang [30] recently

* Corresponding authors. State Key Laboratory for Mechanical Behavior of Materials, Xi'an Jiaotong University, Xi'an 710049, China.
E-mail addresses: wyf7777@c-nin.com (Y.-F. Wu), ynliu@mail.xjtu.edu.cn (Y.-N. Liu), xizp@c-nin.com (Z.-P. Xi).

0378-7753/$ – see front matter © 2014 Elsevier B.V. All rights reserved.
http://dx.doi.org/10.1016/j.jpowsour.2014.01.039

reported micro-nano hierarchical structured $LiFePO_4$/C composite with both superior high-rate performance and high tap density of 1.4 g cm^{-3}. Wei Wei [21] lately synthesized the $LiFePO_4$/C microspheres consisting of closely packed nanosheets showed not only high rate performance and good cycling stability, but also a high tap density of 1.5 g cm^{-3}. Dominko et al. [18] reported that $LiFePO_4$ particles with hierarchically organized pores can operate at current rates up to 50C while still preserving a high tap density of 1.9 g cm^{-3}. Thus, it is significant to explore a reasonable synthetic method for the construction of $LiFePO_4$ hierarchical structures to get an excellent electrochemical performance as well as a high tap density.

In this paper, chemical co-precipitation method has been adopted and the hierarchically constructed nano-grains $LiFePO_4$/C microspheres have been successfully achieved. As we know, the $LiFePO_4$/C microspheres can be synthesized by spray drying method [31,32], ionic liquid solvothermal method [33–35] and chemical co-precipitation method. These three different methods are all kind of liquid methods to get precursor of $LiFePO_4$. However, the spray drying uses hot air as carrier to obtain precursor. The ionic liquid solvothermal method uses autoclave to obtain precursor at high pressure and suitable temperature. The chemical co-precipitation method could get precursor of $LiFePO_4$ at ambient atmosphere and do not apply any carrier. It is proved to be a simple synthesis route for hierarchically $LiFePO_4$/C microspheres in low processing cost with tailored morphology and superior electrochemical performance under soft reaction conditions.

2. Experimental

2.1. Materials and preparation

The precursor powders of $LiFePO_4$ were prepared by chemical co-precipitation method using stoichiometric LiH_2PO_4 (Alfa, 97%), $FeSO_4 \cdot 7H_2O$ (Alfa, 99%) and $LiOH \cdot H_2O$ (Alfa, 98%) as starting materials. The polyethylene glycol (PEG) in molecular weight of 6000 as the dispersant was added to help to form the hierarchical $LiFePO_4$ nano-grain microspheres. The suspension was stirred at 0–4 °C for about 30 min and aged for about 2 h. The final precursor powder product was then filtered, washed with ethanol, and dried at 100 °C in a vacuum oven for 2 h. To obtain $LiFePO_4$/C composites, the precursor powders were well mixed with glucoses and heat treated at the temperature from 950 K to 1025 K at Ar–H_2 atmosphere.

2.2. Characterization

The crystal structure of the precursor powder and the $LiFePO_4$/C composites were investigated by X-ray diffraction (XRD) with Cu Kα radiation on a D8 ADVANCE XRD instrument. The morphology and dimension of the $LiFePO_4$ samples were characterized with a JSM-6460 scanning electron microscope (SEM) and Transmission Electron Microscopy (TEM). The microstructure of the sample was determined using high-resolution transmission electron microscopy (HRTEM) on a JEM-2100 apparatus with an acceleration voltage of 200 kV. Phase and structure of the material were monitored using selected area electron diffraction (SAED). The crystal structure data of $LiFePO_4$ (ICSD #56291) comes from Vestnik Moskovskogo Universiteta, Geologiya (1990), 45, 93–99. The crystal structure data of Fe_2P (ICSD #85561) comes from Annales de Chimie (Paris) (1998), 23, 177–180. The crystal orientation was indexed by the software Singlecrystal 2.0.

The tap density was measured by adding a determinate quantity of the $LiFePO_4$ powder into a measuring cylinder, and then continually tapping the cylinder on a table until no further change of the volume of these powders. The ratio of the mass to the final volume of the powder was taken as the tap density.

2.3. Electrochemical measurement

The working electrode was prepared by 86 wt.% $LiFePO_4$/C composite material, 7 wt.% carbon black and 7 wt.% polyvinylidene fluoride (PVDF) binder. To measure the electric conductivities of these electrodes, they were pasted and pressed on the glass slides. The standard four probe method was carried out by Keithley 181 Nanovoltmeter.

For electrochemical measurements, the working electrode was pasted and pressed on an aluminum foil as the current collector. The carbon contents of the working electrode are about 10 wt.%. It includes the residual carbon of 3 wt.% as decomposed from glucose and 7 wt.% carbon black as conductive additives. The electrochemical properties were measured in cells with metallic lithium as the negative electrode. The electrolyte was 1 M $LiPF_6$ in ethylene carbonate (EC) and diethyl carbonate (DEC). The cells were galvanostatically charged and discharged in the voltage range of 2.0–4.3 V at room temperature using Neware BTS Device.

3. Results and discussion

3.1. Structural and morphology characterization

Fig. 1 shows the XRD pattern of the $LiFePO_4$/C composites treated at different temperatures. Insets are the magnification of XRD patterns with 2 theta from 35 to 51° for the sample treated at 1025 K. The diffraction peaks can be well indexed to be pure $LiFePO_4$ with an orthorhombic olivine structure (JCPDS card No.40-1499) except the appearance of Fe_2P conductive phase (JCPDS card No.33-0670) in the sample treated at 1025 K. The diffraction peaks of $LiFePO_4$ are strong and narrow, indicating the high crystallinity of the $LiFePO_4$ sample. It was observed that Fe_2P, evolved by breakage of the covalent bond between phosphorus and oxygen in the PO_4^{3-} polyanion and bond formation between iron and phosphorus, exists in the $LiFePO_4$/C composite when the sintering temperature is above a critical temperature. Herle et al. and Arnold et al. [36–38] reported the formation of conductive nano-networks of impurity phases (e.g., Fe_2P, Fe_3P) at higher sintering temperatures under reduced conditions which lead to enhanced electrochemical

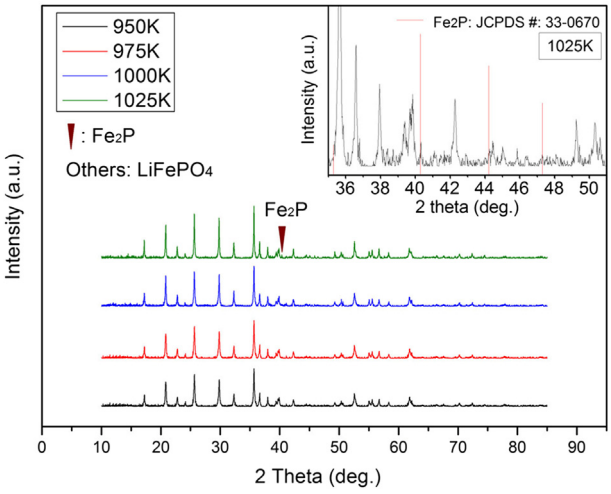

Fig. 1. The XRD pattern of the $LiFePO_4$/C composites treated at different temperatures. Insets: The magnification of XRD patterns with 2 theta from 35 to 51° for the sample treated at 1025 K.

performance of the samples. Therefore, we try to deal with a composite material that contained with Fe_2P phase at elevated temperature with highly resistive nano-grains and electronically conductive surfaces of the grains, which create the conductive paths for the samples. Otherwise, Carbon has not been detected because the residual carbon is amorphous. The residual amorphous carbon mostly comes from the decomposition product of the glucose, but slightly comes from the decomposition product of surfactant PEG after the annealing process. As we know, the surfactant itself remains more or less in the precursor powder of $LiFePO_4$, even after being rinsed many times with distilled water.

Fig. 2 displays the $LiFePO_4$ microspheres by SEM, showing that they are hierarchically constructed with $LiFePO_4$ nano-grains, while these nano-grains are in the size of 20–100 nm in diameter and attached side by side in an ordered fashion. The microspheres formed by these nano-grains are in the size of 1–2 μm. The micron-sized sphere is beneficial for increasing the tap density, as the larger size of the secondary particles (1–2 μm) allows for a denser packing, while the smaller size of the primary grains (20–100 nm) improve Li-ion diffusion rate, which is favorite for the rate capability. It is worth mentioning that these microspheres are sufficiently stable that they cannot be totally destroyed into dispersed nano-grains even after a grinding process.

The bright-field, low-magnification STEM and TEM images of the sample treated at 1025 K are displayed in Fig. 3. The whole microsphere is shown in STEM image in Fig. 3a. Part of the microsphere is shown in TEM image in Fig. 3b, which indicates that the material contains roundish crystallites in the size of 20–100 nm as confirmed by the SEM measurement. The morphologies of carbon coated layer around $LiFePO_4$ are shown in Fig. 4. The low-magnification TEM image shows that the $LiFePO_4$ particles are surrounded uniformly and completely by a carbon coated layer as indicated in Fig. 4a. It can be seen from the HRTEM in Fig. 4b that the carbon coated layer is amorphous and about 2∼3 nm in thickness. The carbon film is thin enough that Li ions can pass from the electrolyte through the film into the solid $LiFePO_4$, where they are stored. It is, of course, the same carbon which simultaneously provides electrons near the spots of Li ion insertion, thus satisfying the material's electroneutrality.

Fig. 5a shows the bright-field TEM images of $LiFePO_4$. The SAED pattern (Fig. 5b), which was obtained along the $[4\bar{1}5]$ zone axis, indicates the diffraction maxima due to reflections from the $(1\bar{1}\bar{1})$ and $(\bar{1}40)$ lattice plane of $LiFePO_4$. The bright zones in the dark-field image (Fig. 5c) represent the grains or subgrains of $LiFePO_4$ which was imaged by diffraction plane $(\bar{1}11)$ circled by the red line in the SAED pattern (Fig. 5b).

Fig. 6 shows the bright-field, dark-field images and SAED pattern of Fe_2P from TEM. The bright-field (Fig. 6a) and dark-field (Fig. 6b) images were obtained in the same area. The SAED pattern (Inset in Fig. 6a) was obtained from the region of the bright-field image circled by the red line. The indexed SAED pattern, which was obtained along the $[1\bar{5}\bar{2}]$ zone axis, indicates the diffraction maxima due to reflections from the $(\bar{2}0\bar{1})$ and $(31\bar{1})$ lattice plane of Fe_2P. The bright zones in Fig. 6b represent Fe_2P phase which was imaged by diffraction plane $(\bar{2}0\bar{1})$ circled by the red line in the SAED pattern (Inset in Fig. 6a). It can be seen from Fig. 6b that the bright zones were distributed at sparse grain boundaries. It is indicated that the Fe_2P phase are distributed at the grain boundary of the $LiFePO_4$.

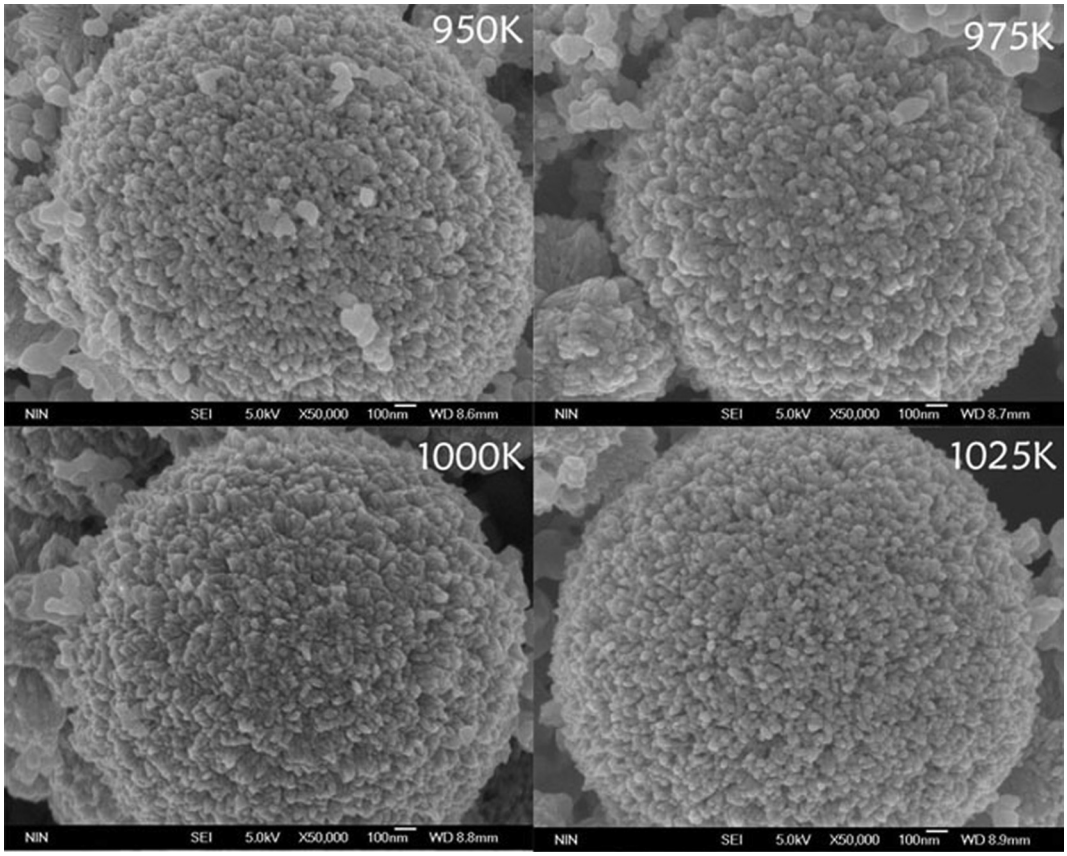

Fig. 2. The morphologies of the $LiFePO_4$/C microspheres treated from 950 K to 1025 K.

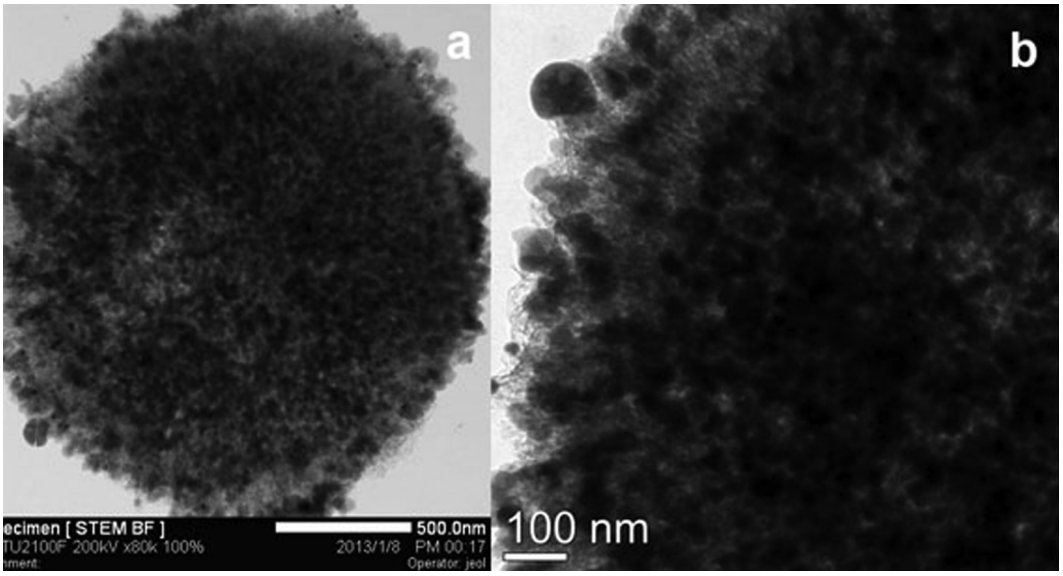

Fig. 3. The bright-field, low-magnification STEM and TEM images of the $LiFePO_4$/C composites.

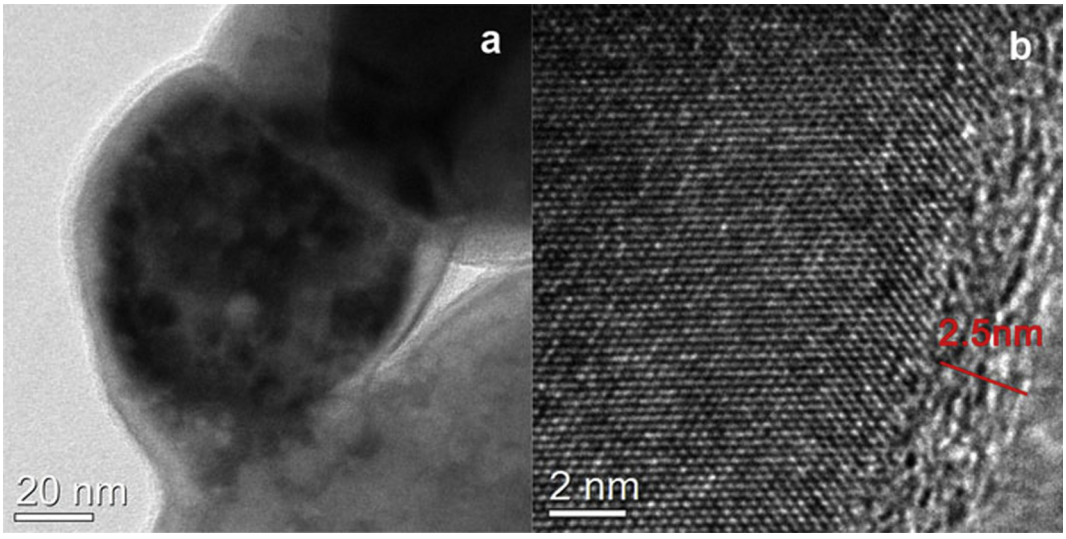

Fig. 4. The amorphous C coated layer in about 2 ~ 3 nm existing for the sample treated at 1025 K.

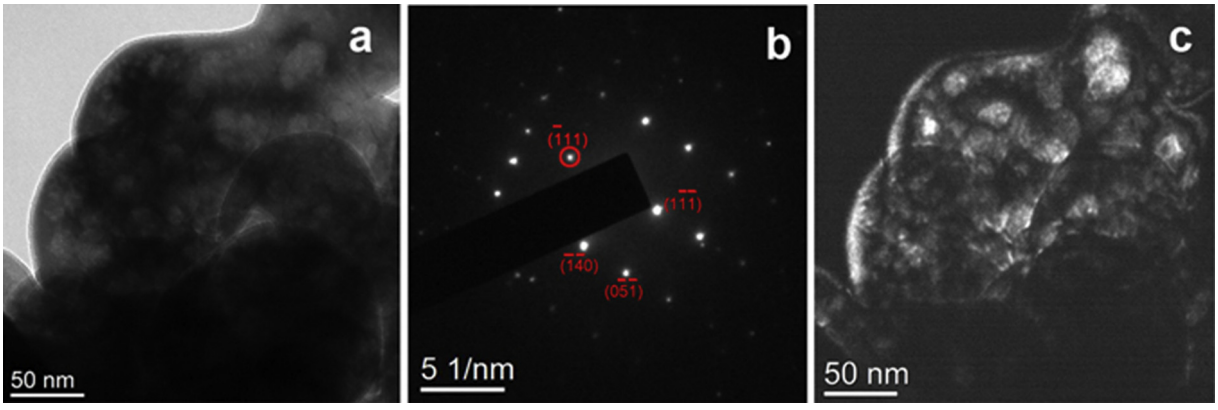

Fig. 5. The bright-field, dark-field TEM images and SAED pattern of $LiFePO_4$.

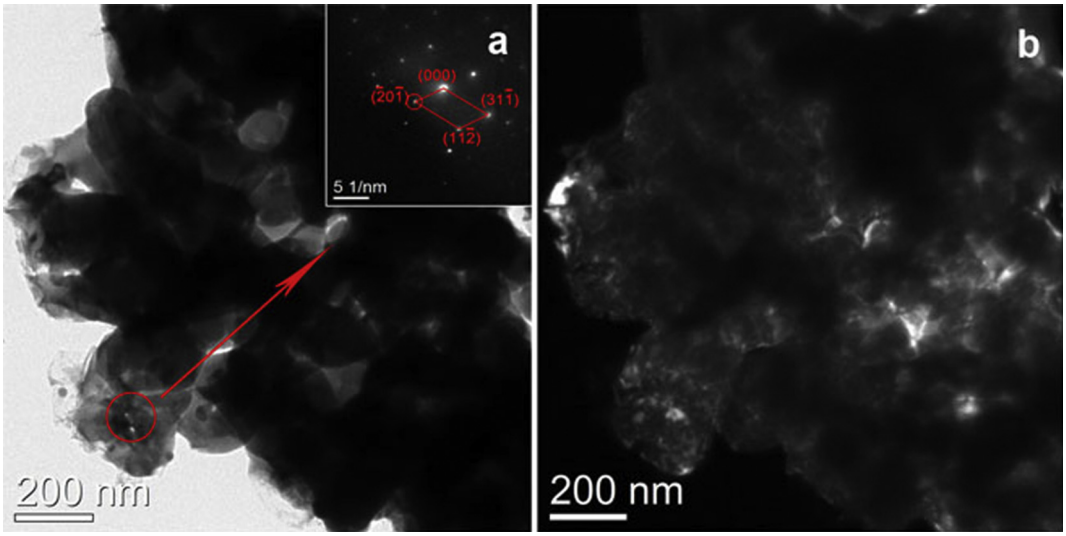

Fig. 6. The bright-field, dark-field TEM images and SAED pattern of Fe_2P.

3.2. Dynamics and electrochemical performance

Fig. 7 shows the electrochemical impedance spectroscopy (EIS) in the frequency range from 0.1 Hz to 100 kHz. The EIS measurements were carried out at different Li-ion intercalation of Li_xFePO_4 for the sample treated at 975 and 1025 K. In the chemical formula of Li_xFePO_4, x represents the amount of Lithium that intercalated into the sample. An EIS spectrum is composed of a semicircle at high-to-middle frequency range and an inclined line within the low frequency range. The resistance of the semicircle is attributed to the charge transfer process. It is indicated in the Fig. 7 that the charge transfer resistance is smaller for the sample treated at 1025 K than that treated at 975 K due to the smaller diameter of the semicircle. Beside conductive carbon, the contained Fe_2P phase in the sample treated at 1025 K creates additional conductive paths from the particle surface to the current collector. The inclined line is attributed to the diffusion of the lithium ions into the bulk of the electrode material, the so-called Warburg diffusion. The Warburg coefficient σ can be obtained by equation [39] (1):

$$Z_{re} = R_e + R_{ct} + \sigma\omega^{-1/2} \quad (1)$$

where R_e is the resistance of the electrolyte, R_{ct} is the charge transfer resistance and ω is the angular frequency in the low frequency region. Both R_e and R_{ct} are kinetics parameters independent of frequency. So σ is the slope for the plot of Z_{re} vs. the reciprocal root square of the lower angular frequencies ($\omega^{-1/2}$). The plot of Z_{re} *vs.* the reciprocal root square of the lower angular frequencies ($\omega^{-1/2}$) at different amounts of intercalation of Li_xFePO_4 for the samples is shown in Fig. 8. The slope of the fitted line is the Warburg coefficient σ. In addition, the Li-ion diffusion rates are determined by the following equation (2) [40]:

$$D = R^2T^2/2A^2n^4F^4C^2\sigma^2 \quad (2)$$

where R is the gas constant, T the absolute temperature (K), F the Faraday constant, A the surface area of the $LiFePO_4$ cathode, n the number of electrons during the process of Li-ion transportation, C the molar concentration of Li-ions in the $LiFePO_4$ cathode and σ the Warburg coefficient. The Warburg coefficient σ and the Li-ion diffusion rates of the samples treated at 975 K and 1025 K are listed in Table 1. The diffusion of the lithium ions into the bulk of the electrode material is becoming difficult when a large amount of Li-ions are intercalated for the sample treated at 975 K. That is why the Warburg coefficient σ is the biggest for the amount of lithium intercalation $x = 0.9$ for this sample. Correspondingly, the Li-ion diffusion rates are remarkably decreased when a large amount of lithium are intercalated into this sample as shown in Table 1. It is

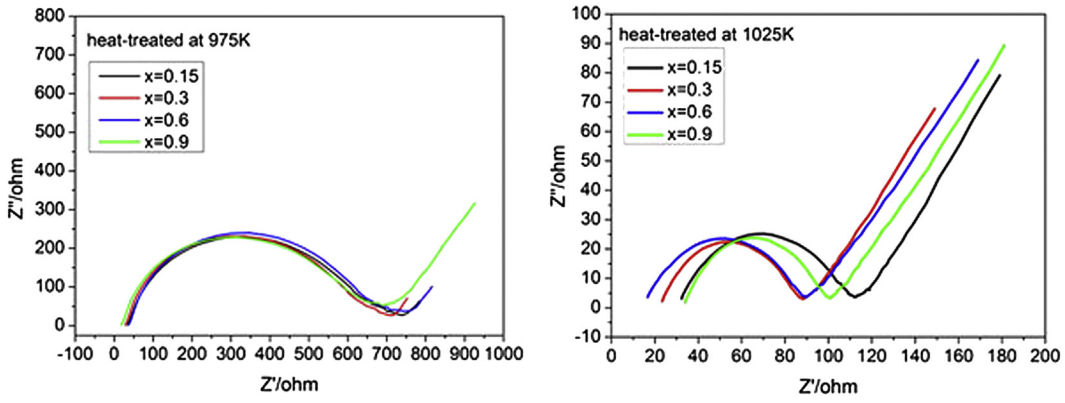

Fig. 7. The electrochemical impedance spectroscopy at different amounts of intercalation of the Li_xFePO_4 for the sample treated at 975 and 1025 K.

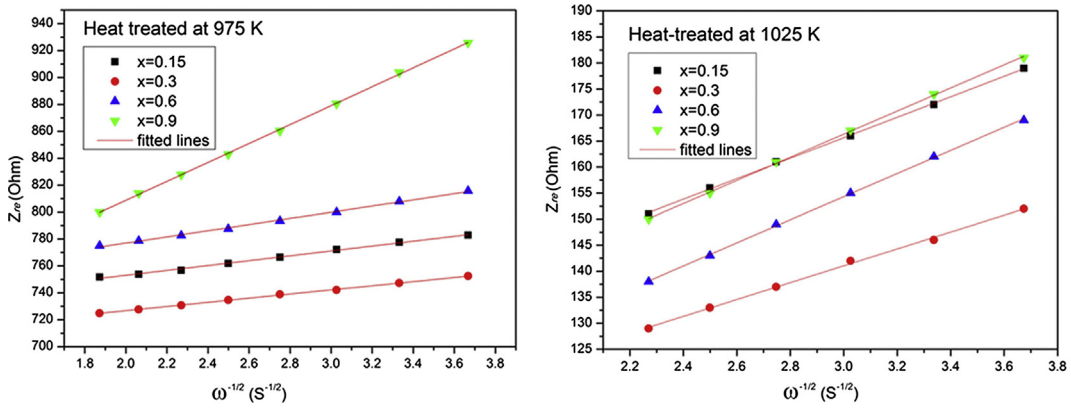

Fig. 8. The plot of Z_{re} *vs*. the reciprocal root square of the lower angular frequencies ($\omega^{-1/2}$) at different amounts of intercalation of Li_xFePO_4 for the sample treated at 975 K and 1025 K.

Table 1
The Warburg coefficient σ and Li-ion diffusion rates (D) for different amounts of lithium intercalation (x) for the sample treated at 975 K and 1025 K.

	x	$x = 0.15$	$x = 0.3$	$x = 0.6$	$x = 0.9$
975 K	σ	18.085	15.862	22.928	68.620
1025 K	σ	19.665	16.188	22.198	22.198
975 K	D ($cm^2\ S^{-1}$)	2.8E-9	8.9E-11	1.1E-11	5.3E-13
1025 K	D ($cm^2\ S^{-1}$)	3.3E-10	1.2E-10	1.6E-11	7.1E-12

noticed that the difference among Warburg coefficient σ is not that big for different amounts of lithium intercalation for the sample treated at 1025 K. Correspondingly, the Li-ion diffusion rates for this sample are limited to 10^{-10}–10^{-12} $cm^2\ S^{-1}$. It is reported [8] that the Li-ion diffusion are 10^{-13}–10^{-16} $cm^2\ S^{-1}$, but it increased to 10^{-9}–10^{-13} $cm^2\ S^{-1}$ as determined by equation (2) in our hierarchically constructed $LiFePO_4$/C nano-grain sample. The Li-ion diffusion rates were improved by hierarchical structured $LiFePO_4$ with small nano-sizes and short Li-transport lengths.

The galvanostatic discharge/charge curves of various heat-treated $LiFePO_4$/C samples at different current rate are presented in Fig. 9. The $LiFePO_4$/C composites show a high discharge capacity of about 160 mAh g^{-1} at the current rate of 0.1C for the samples treated from 950 K to 1000 K, then decreases to 143.4 mAh g^{-1} for the sample treated at 1025 K. It is because the appearance of Fe_2P phase that decreases the content of $LiFePO_4$ phase in this sample. However, its rate capability has been greatly improved. The discharge capacities maintain 139.7, 135.4, 126.1 and 100.0 mAh g^{-1} for this sample at the current rate of 0.5C, 1C, 2C and 5C, respectively. This attributes to its high electric conductivity of 0.09 S cm^{-1} as measured by four probe method. The electric conductivities of the samples treated at different temperatures are showed in

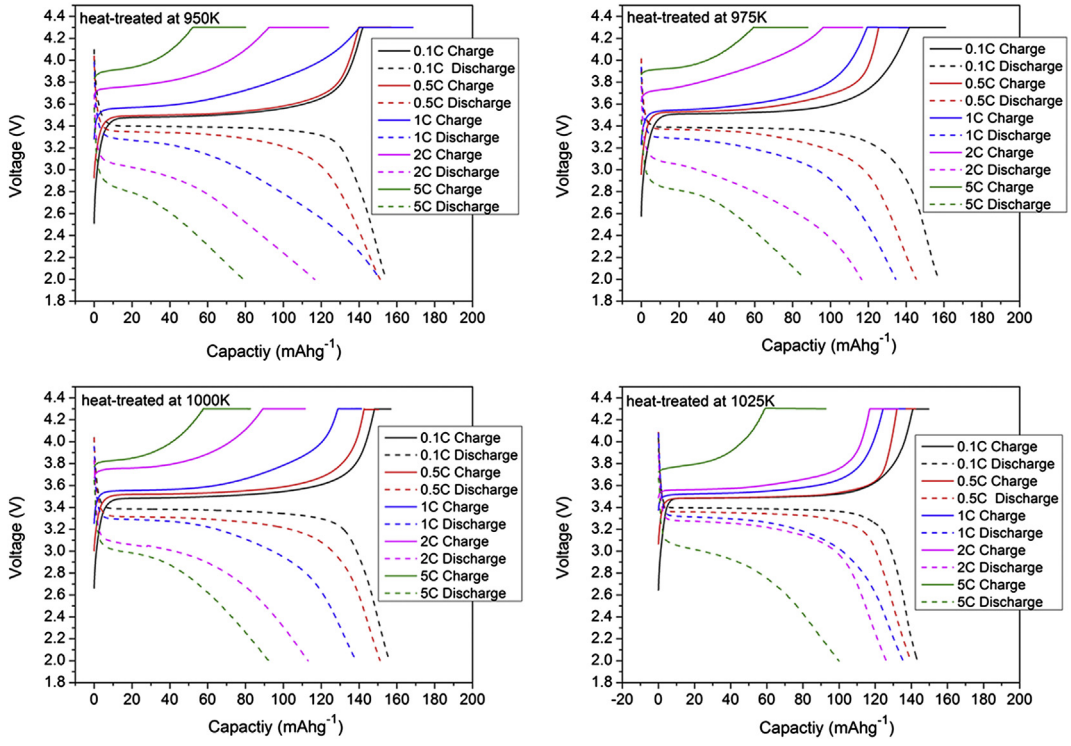

Fig. 9. The initial charge and discharge profiles of various heat-treated $LiFePO_4$/C samples at rates from 0.1C to 5C at room temperature.

Table 2. The electric conductivity was increased by the in-situ formation of Fe_2P phase for the sample treated at 1025 K as confirmed by many literature [41–43].

Flat discharge plateaus at 3.4 V (vs. Li/Li+) are presented in Fig. 9 for all the samples at 0.1C. The potential of the discharge plateau dropped as the rates were increased, which was a result of polarization within the electrode material. The polarization was caused by slow charge transfer due to resistance from the $LiFePO_4$ electrode [44,45]. Upon increasing the current rate, the potential plateau dropped to 3.1 V at the current rate of 2C for samples treated at 950–1000 K. However, the flat potential plateau is retained at 3.3 V for the sample treated at 1025 K even at the current rate of 2C. The small potential polarization of this sample indicates good reaction kinetics, consistent with good high rate capability, which caused by its high electric conductivity induced by in situ formation of Fe_2P.

The Li-ion diffusion rates are significantly increased to 10^{-9}–10^{-13} cm^2 S^{-1} with different amount of intercalation of lithium for the sample treated at 975 K compare to the 10^{-13}–10^{-16} cm^2 S^{-1} as reported in the review paper [8]. The Li-ion diffusion rates are 10^{-10}–10^{-12} cm^2 S^{-1} for the sample treated at 1025 K with different amount of intercalation of lithium as measured in Table 1. It is interesting that the Li-ion diffusion rates are not much different between these two samples since they are all hierarchically constructed $LiFePO_4$/C nano-grains. However, the increases of rate capacities for the sample treated at 975 K are not as obvious as Fe_2P-contained sample that treated at 1025 K. In other words, the rate capacities increased by the Li-ion diffusion rate are not as obvious as the electric conductivity of cathode electrode. It is considered in our paper that the rate capacities increased by Li-ion diffusion rate are not as obvious as electric conductivity. Therefore, the $LiFePO_4$/$FePO_4$ reaction is a non-diffusive controlled process and dynamics do not mainly depend on a diffusion phenomenon associated with a concentration gradient. The Li insertion/extraction process in $LiFePO_4$ appears to take place through the cooperative motion of electrons and Li-ions along the phase boundaries. It means that the transport of Li ions and electrons through the $LiFePO_4$ particles is no longer the limiting process. Alternatively, the fast transport of electrons from the particle surface to the current collector is more crucial, particularly at a high current rate. This viewpoint is further confirmed by the smaller charge transfer resistance as indicated by the smaller diameter of semicircle in Fig. 7 for the sample treated at 1025 K as compared to 975 K. Thus, conductive Fe_2P or carbon loading is more important than particle size control at high current rates.

Fig. 10 shows the discharge capacity vs. cycle number of the samples at the current rate of C/3 in charge and 1C in discharge as measured at room temperature. The capacity retention is above 100% until 300 cycles at the discharge current rate of 1C, indicating that the as-prepared samples can retain good stabilities upon cycling. There is no capacity fading but a slight increase in capacity with increasing cycle number, which demonstrates the excellent cycling stabilities of the hierarchical carbon-coated $LiFePO_4$ nano-grain microspheres. It is worth noting that it is usually very difficult to reach such a high cycling performance for nano-grains with large specific surface area and high reaction activity.

The tap densities of micro-sized $LiFePO_4$ are in the range of 1.0–1.5 g cm^{-3} in the literature [46–49]. The nano-sized $LiFePO_4$ materials have a tap density of 0.6–1.0 g cm^{-3} in the literature [46,50,51]. A low tap density reduces energy density and increases the cell size and cost because more supporting materials such as electrolyte, separator and packaging materials, are needed as a result of less loaded active powders per volume or per area [8]. Although our samples are nano-grains, they form microspheres in micron size. The tap density of our samples was measured to be 1.30 g cm^{-3} with the residual carbon of 3 wt.% as decomposed from glucose, which is comparable to the micro-sized samples. Compared with monodispersed porous $LiFePO_4$ in the literature [35], our $LiFePO_4$ microspheres show a multi-peak particle size distribution as shown in Fig. 11. It is beneficial for improving the tap density of the samples because $LiFePO_4$ microspheres could pack more densely due to the gap filling effect of small particles among large particles. The D50 for $LiFePO_4$ particles are 0.147, 0.157, 0.144 and 0.138 μm for the samples treated at 950–1025 K, respectively. The high rate performances of our samples are also comparable to the monodispersed porous $LiFePO_4$ microspheres. The discharge capacity reaches to 100 mAh g^{-1} and the flat potential plateau is retained at 3.05 V as shown in Fig. 9 for our sample treated at 1025 K even at the current rate of 5C. The high tap density of this special hierarchical microstructure makes the material a promising candidate for use in lithium-ion batteries, as it could greatly increase the energy density of the battery.

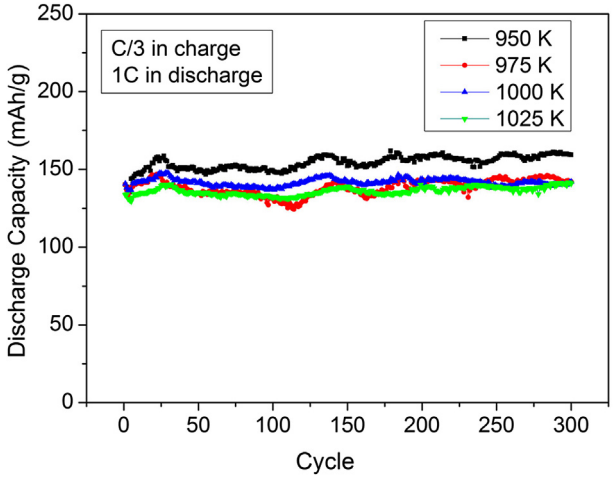

Fig. 10. Discharge capacity vs. cycle number of the samples treated at different temperatures.

Table 2
The electric conductivities of the samples treated at 950–1025 K.

Temperature (K)	950 K	975 K	1000 K	1025 K
Electric conductivity (S cm^{-1})	0.03	0.03	0.05	0.09

4. Conclusion

The chemical co-precipitation method was employed and hierarchically constructed nano-grains $LiFePO_4$/C microspheres were successfully achieved in this paper. The microstructure, dynamics and electrochemical properties of hierarchical $LiFePO_4$/C microspheres that treated at different temperatures were investigated. The Fe_2P conductive phase that distributed at the grain boundary of $LiFePO_4$ contributes much to the electric conductivity and appeared when the temperature is increased to 1025 K. The Li-ion diffusion rates are significantly increased to 10^{-9}–10^{-13} cm^2 S^{-1} by 3–4 order of magnitudes. The hierarchical $LiFePO_4$/C microspheres consisting of primary nano-grains showed not only high discharge capacity (160 mAh g^{-1}) and good cycling stability (up to 300 cycles), but also a high tap density (1.30 g cm^{-3}). All these improved properties proved that the hierarchical LiFePO4/C microspheres prepared by chemical co-precipitation method are the promising candidate for the practical applications in Li-ion batteries.

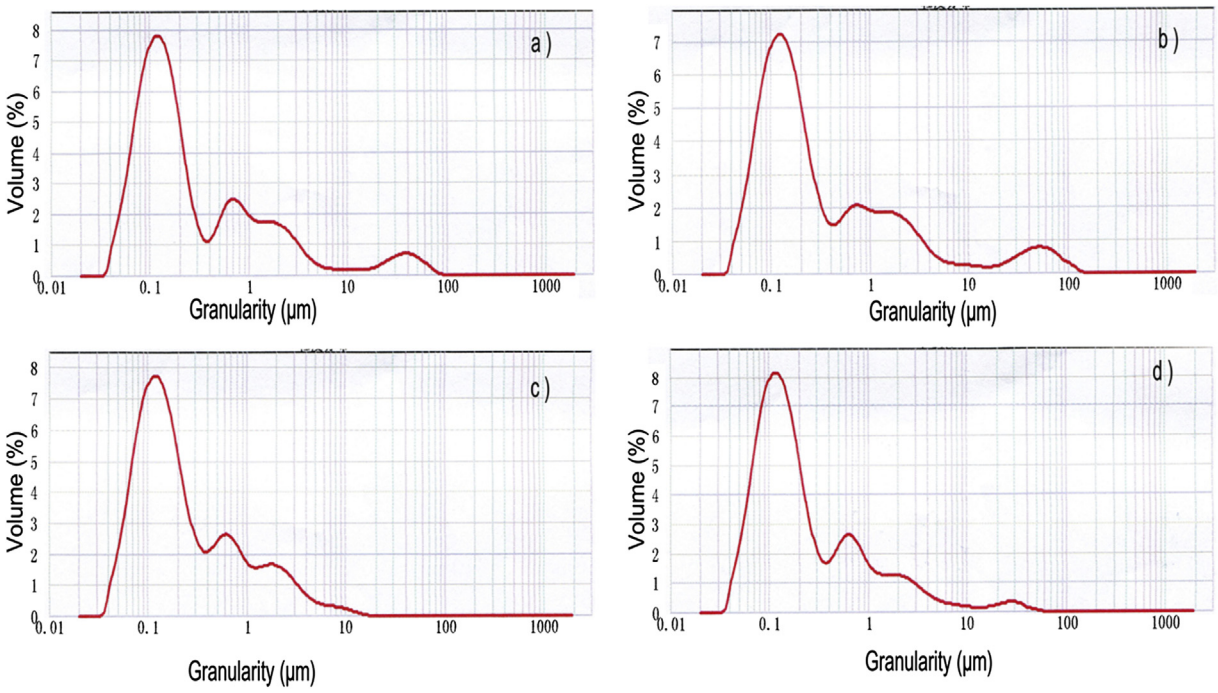

Fig. 11. Size distribution of $LiFePO_4$/C microspheres for the samples treated at different temperatures. a) 950 K, b) 1000 K, c) 1025 K and d) 1050 K.

It is considered in this paper that the rate capacities increased by Li-ion diffusion rate are not as obvious as electric conductivity. Therefore, the $LiFePO_4/FePO_4$ reaction is a non-diffusional controlled process and the reaction dynamics do not mainly depend on a diffusion phenomenon associated with a concentration gradient. The Li insertion/extraction process in $LiFePO_4$ appears to take place through the cooperative motion of electrons and Li-ions along the phase boundaries. It means that the transport of Li ions and electrons through the $LiFePO_4$ particles is no longer the limiting process. Alternatively, the fast transport of electrons from the particle surface to the current collector is more crucial, particularly at a high current rate.

Acknowledgments

This work was partially supported by Industrial Research Project of Science and Technology Department in Shaanxi Province of China (contract no. 2013K09-10).

References

[1] D. Howell, DOE Energy Storage Research and Development, 2008. Annual Progress Report.
[2] A. Ritchie, W. Howard, J. Power Sources 162 (2006) 809.
[3] J.M. Tarascon, M. Armand, Nature 414 (2001) 359.
[4] M.S. Whittingham, MRS Bull. 33 (2008) 411.
[5] T. Ohzuhu, R.J. Brodd, J. Power Sources 174 (2007) 449.
[6] D. Jugovic, D. Uskokovic, J. Power Sources 190 (2009) 538.
[7] B. Scrosati, J. Garche, J. Power Sources 195 (2010) 2419.
[8] Wei-Jun Zhang, J. Power Sources 196 (2011) 2962.
[9] Brian L. Ellis, Kyu Tae Lee, Linda F. Nazar, Chem. Mater. 22 (2010) 691.
[10] K.H. Rhodes, S.A. Davis, F. Caruso, B. Zhang, S. Mann, Chem. Mater. 12 (2000) 2832.
[11] F. Kim, S. Kwan, J. Akana, P. Yang, J. Am. Chem. Soc. 123 (2001) 4360.
[12] X. Fan, X.M. Meng, X.H. Zhang, W.S. Shi, W.J. Zhang, J.A. Zapien, C.S. Lee, S.T. Lee, Angew. Chem. Int. Ed. 45 (2006) 2568.
[13] J. Wu, F. Duan, Y. Zheng, Y. Xie, J. Phys. Chem. C 111 (2007) 12866.
[14] X. Zhang, Z. Ai, F. Jia, L. Zhang, J. Phys. Chem. C 112 (2008) 747.
[15] B. Ellis, W.H. Kan, W.R.M. Makahnouk, L.F. Nazar, J. Mater. Chem. 17 (2007) 3248.
[16] P.P. Prosini, M. Carewska, S. Scaccia, P. Wisniewski, S. Passerini, M. Pasquali, J. Electrochem. Soc. 149 (2002) A886.
[17] H. Huang, S.C. Yin, L.F. Nazar, Electrochem. Solid-State Lett. 4 (2001) A170.
[18] R. Dominko, M. Bele, J.M. Goupil, M. Gaberscek, D. Hanzel, I. Arcon, J. Jamnik, Chem. Mater. 19 (2007) 2960.
[19] Y.S. Hu, Y.G. Guo, R. Dominko, M. Gaberscek, J. Jamnik, J. Maiar, Adv. Mater. 19 (2007) 1963.
[20] Yongmin Wu, Zhenhai Wen, Jinghong Li, Adv. Mater. 23 (2011) 1126.
[21] Wei Wei, Dezhi Chen, Ruining Wang, Lin Guo, Nanotechnology 23 (2012) 475401.
[22] A. Magasinski, P. Dixon, B. Hertzberg, A. Kvit, J. Ayala, G. Yushin, Nat. Mater. 9 (2010) 353.
[23] Y.S. Hu, P. Adelhelm, B.M. Smarsly, S. Hore, M. Antonietti, J. Maier, Adv. Funct. Mater. 17 (2007) 1873.
[24] F.F. Tao, C.C. Gao, Z.H. Wen, Q. Wang, J.H. Li, Z. Xu, J. Solid State Chem. 182 (2009) 1055.
[25] Z.H. Wen, J.H. Li, J. Mater. Chem. 19 (2009) 8707.
[26] W. Zhou, M. Yao, L. Guo, Y.M. Li, J.H. Li, S.H. Yang, J. Am. Chem. Soc. 131 (2009) 2959.
[27] Q. Wang, Z.H. Wen, J.H. Li, J. Power Sources 334 (2008) 182.
[28] K.R. Saravanan, M.V. Reddy, P. Balaya, H. Gong, B.V.R. Chowdari, J.J. Vittal, J. Mater. Chem. 19 (2009) 605.
[29] K.R. Saravanan, P. Balaya, M.V. Reddy, B.V.R. Chowdari, J.J. Vittal, Energy Environ. Sci. 3 (2010) 457.
[30] Meng Wang, Yong Yang, Youxiang Zhang, Nanoscale 3 (2011) 4434.
[31] Feng Yu, Jingjie Zhang, Yanfeng Yang, Guangzhi Song, J. Power Sources 189 (2009) 794.
[32] Jiali Liu, Zhangzhi Wang, Guohua Zhang, Yun Liu, Aishui Yu, Int. J. Electrochem. Sci. 8 (2013) 2378.
[33] Binbin Guo, Hongcheng Ruan, Cheng Zheng, Hailong Fei, Mingdeng Wei, Sci. Rep. 3 (2013) 2788.
[34] Bing Sun, Ying Wang, Bei Wang, Hyun-Soo Kim, Woo-Seong Kim, Guoxiu Wang, J. Nanosci. Nanotechnol. 13 (2013) 3655.
[35] Chunwen Sun, S. Rajasekhara, J.B. Goodengough, Feng Zhou, J. Am. Chem. Soc. 133 (2011) 2132.
[36] G. Arnold, J. Garche, R. Hemmer, S. Ströbele, C. Vogler, M. Wohlfahrt-Mehrens, J. Power Sources 247 (2003) 119.
[37] S.P. Herle, B. Ellis, N. Coombs, L.F. Nazar, Nat. Mater. 3 (2004) 147.
[38] Sung-yoon Chung, T. Jason Bloking, Yet-ming Chiang, Nat. Mater. 1 (2002) 123.
[39] Yan Cui, Zhao Xiaoli, Guo Ruisong, Electrochim. Acta 55 (2010) 922.
[40] Lian-liang Wang, Pei-hua Ma, Kun Zhang, Cheng-hua Gao, Chun-yan Yan, J. Salt Lake Res. 17 (2009) 52.
[41] Cheol Woo Kim, Jong Suk Park, Kyung Sub Lee, J. Power Sources 163 (2006) 144.
[42] Youyong Liu, Chuanbao Cao, Jing Li, Xingyan Xu, J. Appl. Electrochem. 40 (2010) 419.
[43] Min-Sang Song, Dong-Yung Kim, Yong-Mook Kang, Yong-Il Kim, Jai-Young Lee, Hyuk-Sang Kwon, J. Power Sources 180 (2008) 546.
[44] D. Choi, P.N. Kumta, J. Power Sources 163 (2007) 1064.
[45] C.H. Mi, X.G. Zhang, X.B. Zhao, H.L. Li, J. Alloys Compd. 424 (2006) 327.

[46] Z.R. Chang, H.J. Lv, H.W. Tang, H.J. Li, X.Z. Yuan, H. Wang, Electrochem. Acta 54 (2009) 4595.
[47] J.M. Chen, C.H. Hsu, Y.R. Lin, M.H. Hsiao, G.T. Fey, J. Power Sources 184 (2008) 498.
[48] J.F. Ni, H.H. Zhou, J.T. Chen, X.X. Zhang, Mater. Lett. 61 (2007) 1260.
[49] L.Q. Sun, R.H. Cui, A.F. Jalbout, M.J. Li, X.M. Pan, R.S. Wang, H.M. Xie, J. Power Sources 189 (2009) 522.
[50] S.T. Yang, N.H. Zhao, H.Y. Dong, J.X. Yang, H.Y. Yue, Electrochem. Acta 51 (2005) 166.
[51] J. Ying, M. Lei, C. Jiang, C. Wan, X. He, J. Li, L. Wang, J. Ren, J. Power Sources 158 (2006) 543.